Supporting Information for

Construction of fluorescent probe for selectively detecting singlet oxygen with high sensitivity and large concentration range based on two-step cascade sensing reaction

Lingliang Long,*[a] Xiangqi Yuan,[a] Siyu Cao,[a] Yuanyuan Han,[a] Weiguo Liu,[a] Qian Chen,[a] Aihua Gong,*[b] and Kun Wang*[a,c]

[a] School of Chemistry and Chemical Engineering, Jiangsu University, Zhenjiang, Jiangsu 212013 (P. R. China).
[b] School of Medicine, Jiangsu University, Zhenjiang, Jiangsu 212013, (P. R. China).
[c] Key Laboratory of Optic-electric Sensing and Analytical Chemistry for Life Science, Ministry of Education, College of Chemistry and Molecular Engineering, Qingdao University of Science and Technology, Qingdao, Shandong 266042 (P. R. China).

Email: longlingliang@163.com; ahg5@ujs.edu.cn; wangkun@ujs.edu.cn

1. Materials and Instruments

Unless otherwise stated, all reagents were purchased from commercial suppliers and used without further purification. Twice-distilled water was used throughout all experiments. Solvents were purified and dried by standard methods prior to use. The RAW 264.7 and PC12 cells were purchased from the Type Culture Collection of the Chinese Academy of Sciences, Shanghai, China. Melting points of compounds were measured on a Beijing Taike XT-4 microscopy melting point apparatus, and all melting points were uncorrected. TLC analyses were performed on silica gel plates and column chromatography was conducted over silica gel (mesh 200-300), both of which were obtained from the Qingdao Ocean Chemicals. ^{1}H and ^{13}C-NMR spectra were recorded on a Bruker Avance 400 spectrometer operating at 400 MHz and 100 MHz respectively. Mass spectra were recorded on a LXQ Spectrometer (Thermo Scientific) operating on ESI. The pH measurements were performed with a pH-3c digital pH-meter (Shanghai ShengCi Device Works, Shanghai, China) with a combined glass-calomel electrode. Electronic absorption spectra were obtained on a SHIMADZU UV-2450 spectrometer. Fluorescence spectra were measured on a Photon Technology International (PTI) Quantamaster fluorometer with 2 nm excitation and emission slit widths. Confocal fluorescence microcopy imaging experiments were performed on a Leica TCS SP5 II laser confocal scanning microscope.

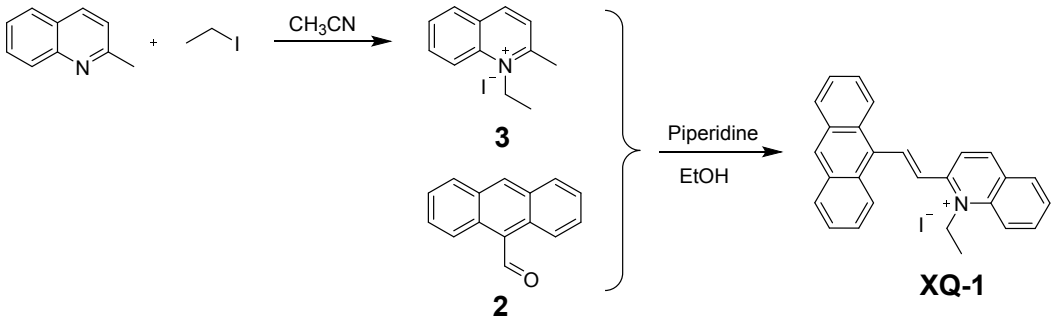

Scheme S1. The synthetic procedure of probe **XQ-1**.

2. Synthesis of N-ethyl-2-methylquinolinium iodide (3)

2-methylquinoline (1.00 g, 6.98 mmol) was added to a solution of ethyl iodide (8.71 g, 55.87 mmol) in CH_3CN (3 mL). Then, the mixture was heated at reflux for 12 hours. After cooling to room temperature, the mixture was filtered and the crude product was recrystallized from CH_2Cl_2 and petroleum ether to afford the green solid (0.96 g, yield 46.0 %). Mp: 242-244 ^oC. ^1H NMR (DMSO-d_6, 400 MHz), δ (ppm): 9.12 (d, J = 8.4 Hz, 1H), 8.63 (d, J = 8.8 Hz, 1H), 8.43 (dd, J = 1.6 Hz, 8.4 Hz, 1H), 8.25 (m, 1H), 8.15 (d, J = 8.4 Hz, 1H), 8.01 (t, J = 7.6 Hz, 1H), 5.01 (q, J = 7.2 Hz, 2H), 3.13 (s, 3H), 1.54 (t, J = 7.2 Hz, 3H). MS (ESI) m/z 172.11 $[M]^+$.

3. Synthesis of probe XQ-1

9-Anthraldehyde (0.50 g, 2.42 mmol) and *N*-ethyl-2-methylquinolinium iodide (0.63 g, 2.10 mmol) were dissolved in 5 mL anhydrous ethanol. Then, piperidine (0.10 g, 1.21 mmol) was added and the mixture was heated at reflux for 10 hours under a nitrogen atmosphere. After cooling to room temperature, the solvent was evaporated off under reduced pressure. The resulting residue was purified by column chromatography (CH_2Cl_2: petroleum ether = 1:1, v/v), yielding a red solid (0.47 g, yield 45.9%). Mp: 223-225 ^oC. ^1H NMR (DMSO-d_6, 400 MHz), δ (ppm): 9.29 (d, J = 8.8 Hz, 1H), 9.10 (d, J = 16.0 Hz, 1H), 9.00 (d, J = 8.8 Hz, 1H), 8.79 (s, 1H), 8.67 (d, J = 9.2 Hz, 1H), 8.51 (m, 3H), 8.27 (m, 1H), 8.22 (m, 2H), 8.05 (t, J = 7.6 Hz, 1H), 7.82 (d, J = 16 Hz, 1H), 7.65 (m, 4H), 5.11 (q, J = 7.2 Hz, 2H), 1.56 (t, J = 7.2 Hz, 3H). ^{13}C NMR (DMSO-d_6, 100 MHz), δ (ppm): 155.5, 145.5, 144.6, 138.4, 136.0, 131.4, 131.0, 130.2, 129.8, 129.7, 129.5, 129.4, 129.2, 128.5, 127.4, 126.3, 125.8, 122.9, 119.5, 47.7, 14.7. MS (ESI) m/z 360.28 $[M]^+$.

4. Detection of $^1O_2$ in aqueous solution

The $^1O_2$ was generated from a Na_2MoO_4/H_2O_2 system[1] and photoirradiation of photosensitizer tetra-(N-methyl-4-pyridyl)porphyrin (**TMPyP4**),[2] respectively. The detailed experimental procedures are as follows:

(1) The reaction of the probe **XQ-1** with $^1O_2$ generated from a Na_2MoO_4/H_2O_2 system was performed in 50 mM carbonate buffer/ EtOH (1: 1 v/v, pH 10.5). Various concentrations of H_2O_2 solutions were added to the buffer solutions containing 200 μM of the probe **XQ-1** and 1.0 mM of Na_2MoO_4. After stirring for 2 h at room temperature, the solutions were 10-fold diluted with 50 mM potassium phosphate buffer/ EtOH (1: 1 v/v, pH 7.4). Then, the fluorescence emission spectra of the solutions were measured.

(2) The reaction of the probe **XQ-1** with $^1O_2$ generated from photoirradiation of photosensitizer **TMPyP4** was performed in 50 mM potassium phosphate buffer / EtOH (1: 1 v/v, pH 7.4). The probe **XQ-1** (20 μM) and **TMPyP4** (5 μM) were co-dissolved in the buffer solution (5 mL). A white LED lamp (150 mW/cm^2) was used as a light source to continuously irradiate **TMPyP4**. Then, the fluorescence emission spectra of the solutions were measured at different time intervals.

5. Reactions of probe XQ-1 with various other ROS, biological molecules, and metal ions

Solutions of the various other reactive oxygen species (ROS), biological molecules, and metal ions were prepared from 5.2% NaClO, 30% H_2O_2, GSH, Cys, $MgCl_2{\cdot}6H_2O$, $FeSO_4{\cdot}7H_2O$, $Fe(NO_3)_3{\cdot}9H_2O$, $CuCl_2{\cdot}2H_2O$ and $Zn(NO_3)_2{\cdot}6H_2O$ respectively. Hydroxyl radical was generated by Fenton reaction.[3] Nitric oxide was generated from SNP (sodium nitroferricyanide (III) dihydrate).[4] All the reactions were carried out in 50 mM potassium phosphate buffer / EtOH (1: 1 v/v, pH 7.4). Probe **XQ-1** (20 μM) was incubated with 0.6 mM various species for 2 hours in the buffer solution at room temperature. Subsequently, the fluorescence emission spectra of the solutions were measured.

6. Determination of fluorescence quantum yield

Fluorescence quantum yield was determined using the solutions of anthracene (Φ_F = 0.30 in ethanol)[5] as a standard. The quantum yield was calculated using the following equation:[6]

$$\Phi_{F(X)} = \Phi_{F(S)} (A_S F_X / A_X F_S) (n_X / n_S)^2$$

Where Φ_F is the fluorescence quantum yield, A is the absorbance at the excitation wavelength, F is the area under the corrected emission curve, and n is the refractive index of the solvents used. Subscripts S and X refer to the standard and to the unknown, respectively.

7. Determination of the detection limit

The detection limit was calculated according to a method used in the literature.[7] The fluorescence emission spectrum of probe **XQ-1** was measured five times and the standard deviation of a blank measurement was achieved. The fluorescence intensity (I_{412}) was plotted as a concentration of $^1O_2$. The detection limit was calculated using the following equation:

$$\text{Detection limit} = 3\,\sigma / k$$

Where σ is the standard deviation of blank measurement, k is the slope between the fluorescence intensity (I_{412}) versus $^1O_2$ concentration.

8. Fluorescence imaging of endogenous $^1O_2$ in RAW 264.7 macrophage cells

The RAW 264.7 cells were seeded in a 24-well plate in Dulbecco's modified Eagle's medium (DMEM) supplemented with 10% fetal bovine serum for 24 h. The cells were stained with probe **XQ-1** (2 μM) in the culture medium for 30 min at 37°C. Then, the cells were stimulated with 0, 5, and 20 μM phorbol 12-myristate 13-acetate (PMA) for 30 min. As a control experiment, the cells were pre-treated with 100 μM histidine for 30 min, followed by PMA (20 μM) stimulation for 30 min. The cells were then washed with PBS buffers three times. Subsequently, fluorescent images were acquired on a Leica TCS SP5 II laser confocal scanning microscope with an objective lens (×40). Blue Channel was set at 420-450 nm with excitation at 405 nm. Green Channel was set at 475-575 nm with excitation at 405 nm.

9. Fluorescence imaging of intracellular $^1O_2$ during the simulated PDT process

PC12 cells were seeded in a 24-well plate in Dulbecco's modified Eagle's medium (DMEM) supplemented with 10% fetal bovine serum for 24 h. After incubated with 5-ALA (150 μg ml^{-1}) for 12 hours to biosynthesize photosensitizer protoporphyrin IX (PpIX), the cells were stained with probe **XQ-1** (2 μM) for 30 min. Then the selected cell region was irradiated with 405 nm laser (20% laser power) to generate $^1O_2$. Meanwhile, the fluorescent images were acquired at different time interval on a Leica TCS SP5 II laser confocal scanning microscope with an objective lens (×10). Blue Channel was set at 420-450 nm with excitation at 405 nm. Green Channel was set at 475-575 nm with excitation at 405 nm.

10. Computational details

The UV/Vis absorption and the emission properties of probe **XQ-1** and compound **2** were studied with DFT/TDDFT calculations at the B3LYP/6-31G(d,p)/level using Gaussian 09.[8] First, the optimized ground-state geometries of probe **XQ-1** and compound **2** were obtained. The UV/Vis absorption was calculated by the TDDFT method based on the ground-state geometry (vertical excitation, Franck-Condon principle). The geometry of excited state was optimized and the emission was calculated with the TDDFT method (usually excited state is responsible for the fluorescence, Kasha's role). The vertical excitation and the emission related calculations were based on the optimized excited state.

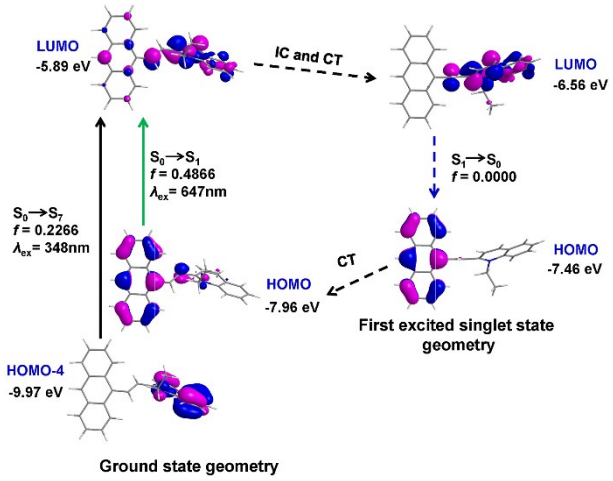

Figure S1. Rationalization of the UV/Vis absorption and the no fluorescence of probe **XQ-1**: the geometry relaxation upon photoexcitation and the frontier molecular orbitals (MOs) involved in the vertical excitation (i.e., UV/Vis absorption, the left columns) and emission (right column) of probe **XQ-1**. The vertical excitations were calculated based on the optimized ground state geometry, the emission was calculated based on the optimized geometry of the excited state. IC stands for internal conversion and CT stands for conformation transformation. Excitation and radiative processes are marked by a solid arrow and the non-radiative processes are marked by dotted arrows.

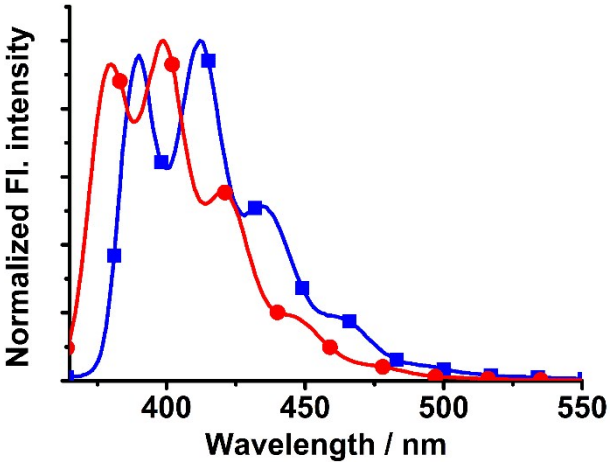

Figure S2. The normalized fluorescence emission spectra of probe **XQ-1** (20 μM) with 0.6 mM $^1O_2$ (λ_{ex} = 368 nm) (■) and anthracene **4** (λ_{ex} = 350 nm) (●). The $^1O_2$ was generated from a Na_2MoO_4/H_2O_2 system.

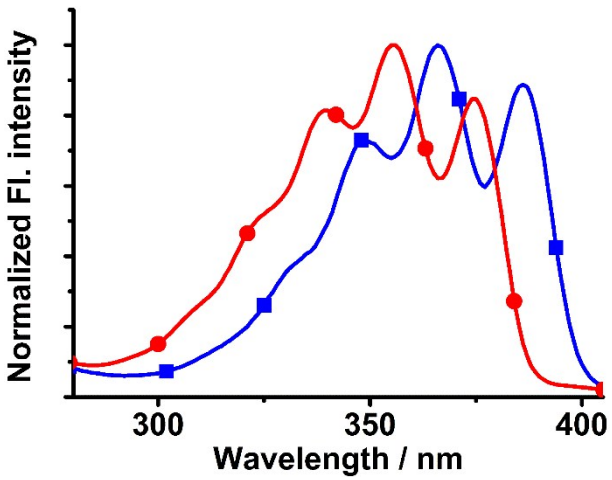

Figure S3. The normalized fluorescence excitation spectra of probe **XQ-1** (20 μM) with 0.6 mM $^1O_2$ (λ_{em} = 412 nm) (■) and anthracene **4** (λ_{em} = 420 nm) (●). The $^1O_2$ was generated from a Na_2MoO_4/H_2O_2 system.

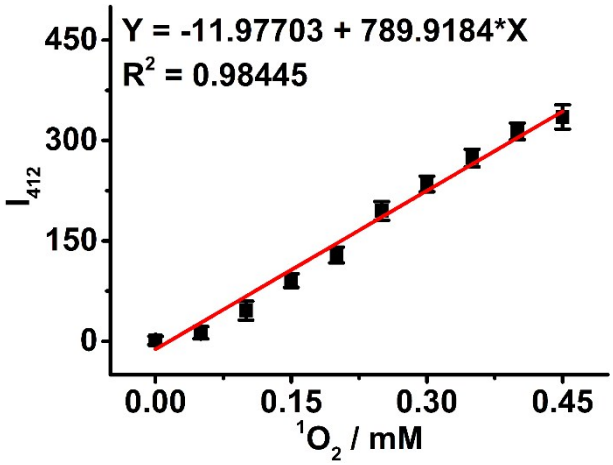

Figure S4. The linear relationship of fluorescence intensity (I_{412}) of probe **XQ-1** (20 μM) to various dosage of $^1O_2$ (0 to 0.45 mM). The $^1O_2$ was generated from a Na_2MoO_4/H_2O_2 system. The error bars represent the standard deviation (n = 3).

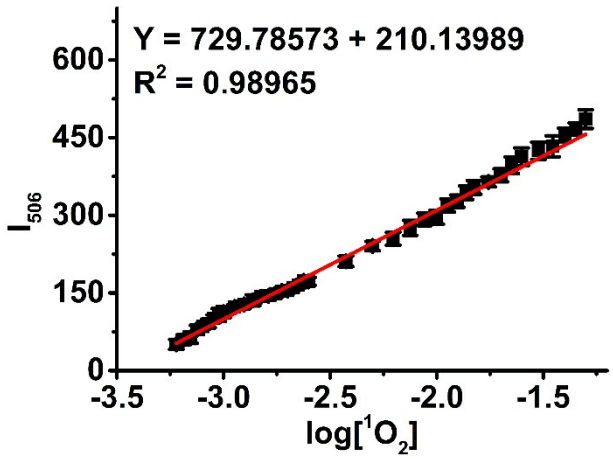

Figure S5. The linear relationship of fluorescence intensity (I_{506}) of probe **XQ-1** (20 μM) to the logarithm of various dosage of $^1O_2$ (0.6 to 50 mM). The $^1O_2$ was generated from a Na_2MoO_4/H_2O_2 system. The error bars represent the standard deviation (n = 3).

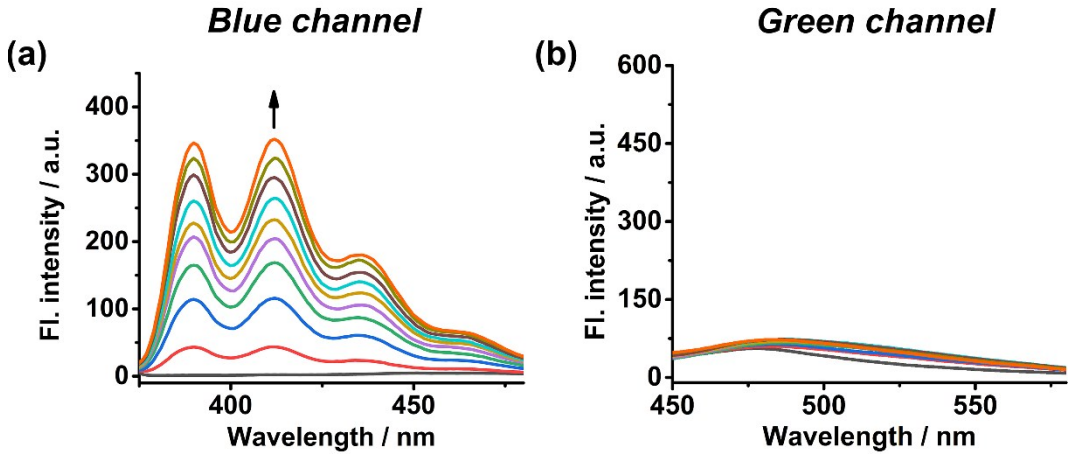

Figure S6. Fluorescence changes in blue channel (λ_{ex} = 368 nm) (a) and green channel (λ_{ex} = 420 nm) (b) of probe **XQ-1** (20 μM) in 50 mM potassium phosphate buffer / EtOH (1: 1 v/v, pH 7.4) upon photoirradiation of co-dissolved **TMPyP4** from 0 second to 80 second.

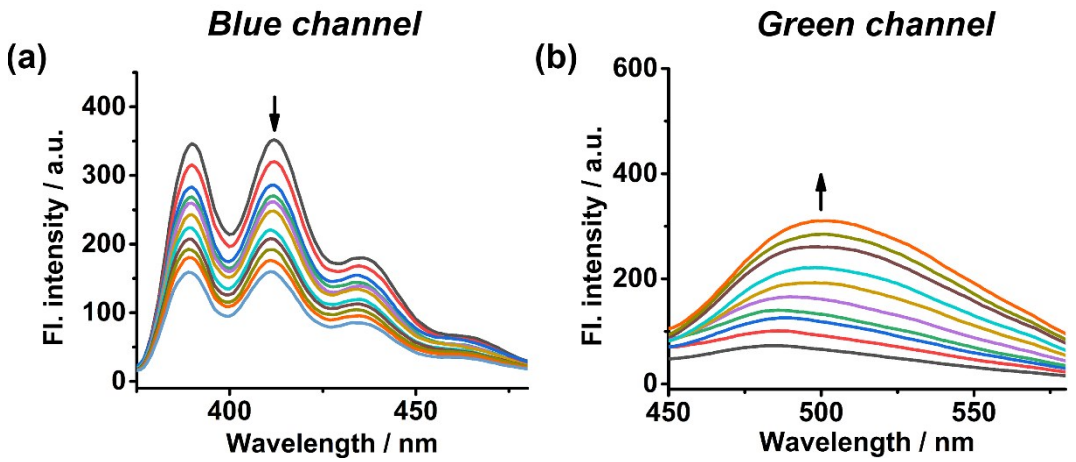

Figure S7. Fluorescence changes in blue channel (λ_{ex} = 368 nm) (a) and green channel (λ_{ex} = 420 nm) (b) of probe **XQ-1** (20 μM) in 50 mM potassium phosphate buffer / EtOH (1: 1 v/v, pH 7.4) upon photoirradiation of co-dissolved **TMPyP4** from 80 second to 40 min.

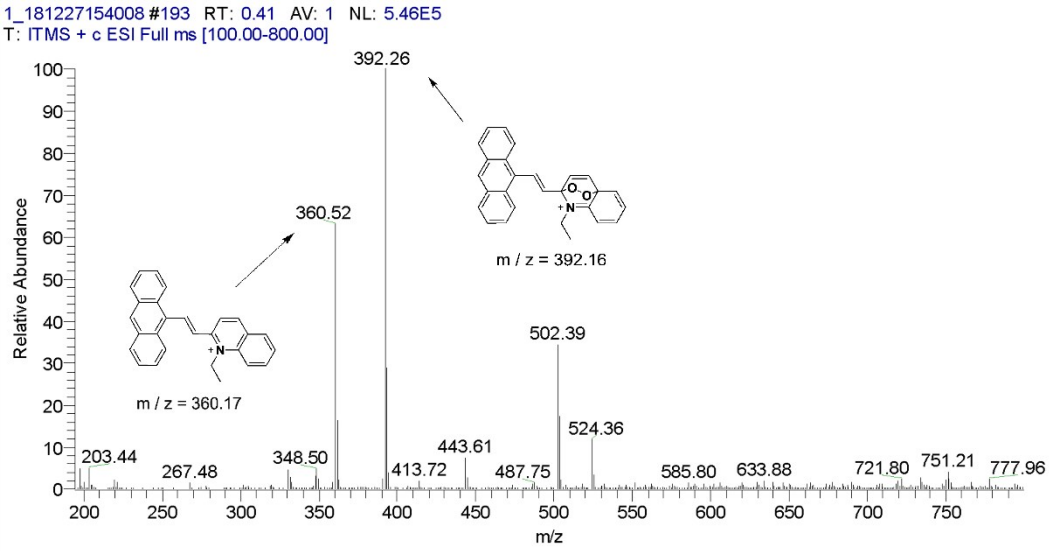

Figure S8. The ESI-Ms spectra of the probe **XQ-1** with $^1O_2$ in the period of first step sensing reaction.

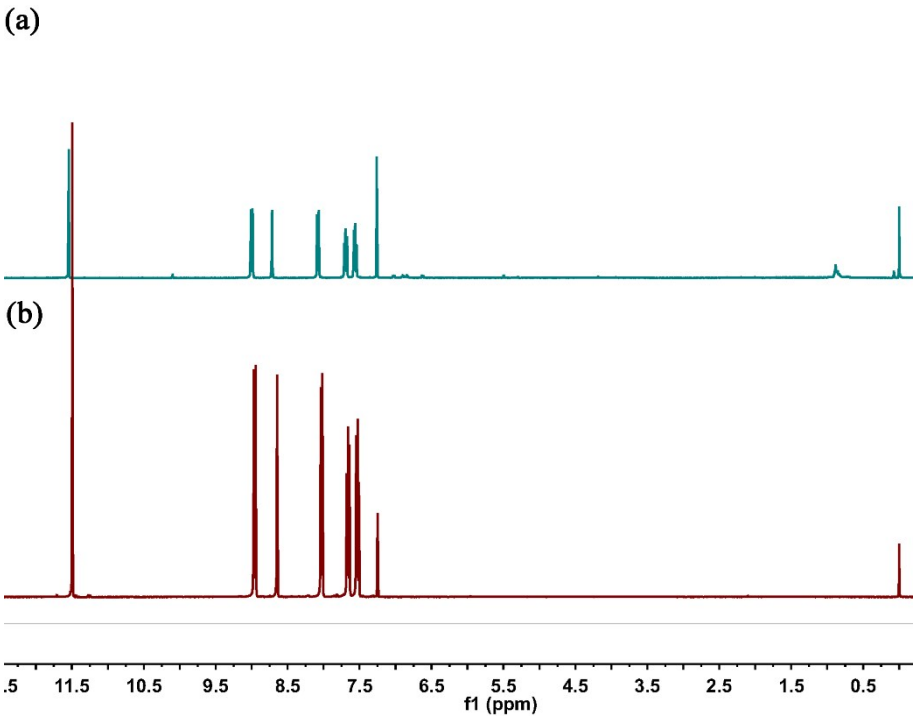

Figure S9. (a) The ^{1}H NMR spectra for the isolated product of probe **XQ-1** with $^{1}O_2$ in the period of second step sensing reaction; (b) the standard ^{1}H NMR spectra for 9-anthraldehyde **2**. The solvent for ^{1}H NMR spectra was $CDCl_3$.

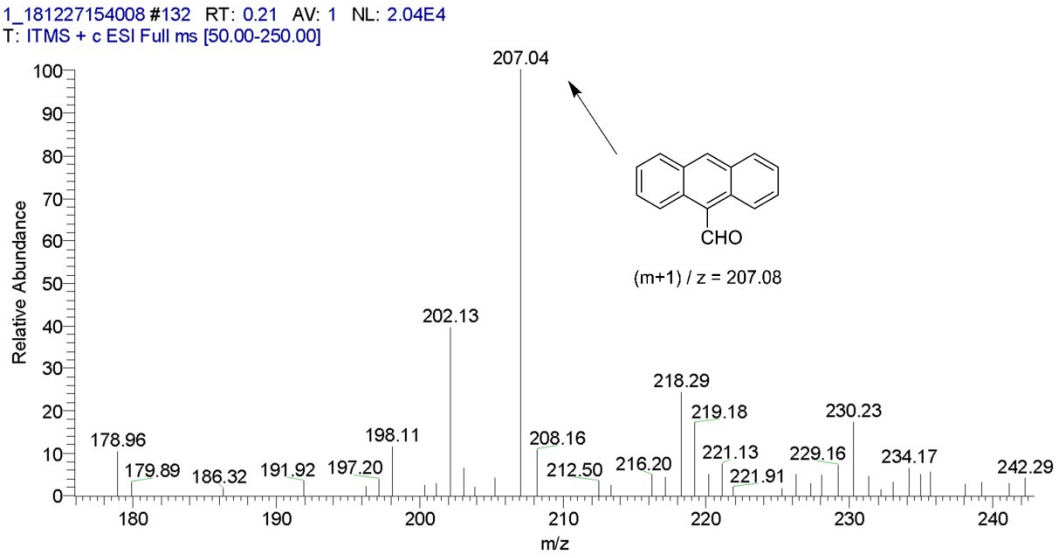

Figure S10. ESI-Ms spectra of the isolated product of probe **XQ-1** with $^{1}O_2$ in the period of second step sensing reaction.

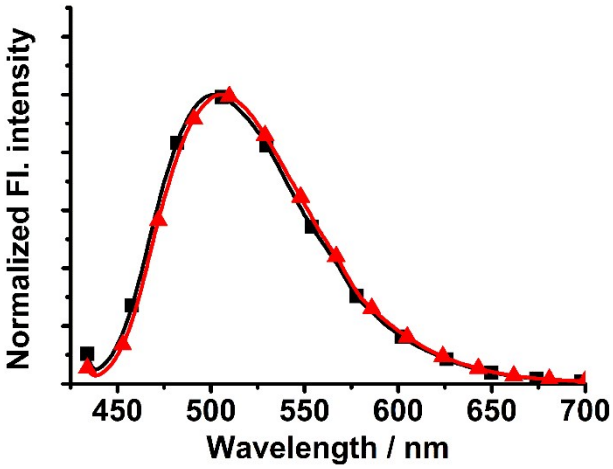

Figure S11. The comparison of normalized fluorescence emission spectra of the isolated product of probe **XQ-1** with $^1O_2$ in the period of second step sensing reaction (■) and 9-Anthraldehyde **2** (▲). The excitation wavelength was 420 nm.

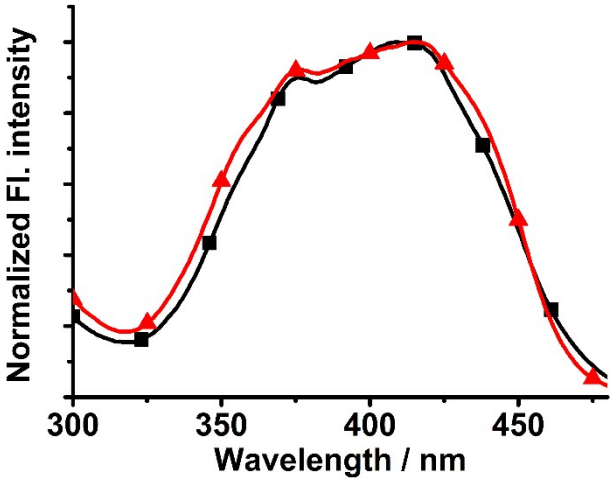

Figure S12. The comparison of normalized fluorescence excitation spectra of the isolated product of probe **XQ-1** with $^1O_2$ in the period of second step sensing reaction (■) and 9-Anthraldehyde **2** (▲) (λ_{em} = 506 nm).

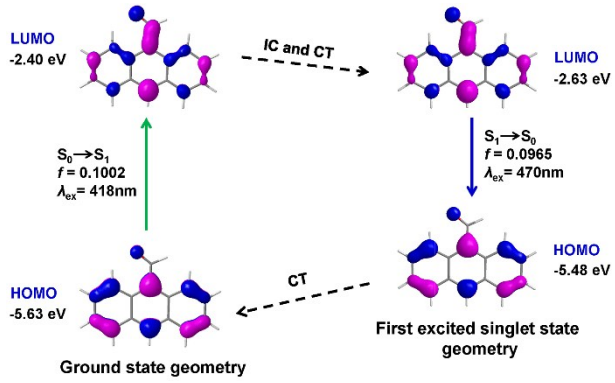

Figure S13. Rationalization of the UV/Vis absorption and the fluorescence of compound **2**: the geometry relaxation upon photoexcitation and the frontier molecular orbitals (MOs) involved in the vertical excitation (i.e., UV/Vis absorption, the left columns) and emission (right column) of compound **2**. The vertical excitations were calculated based on the optimized ground state geometry; the emission was calculated based on the optimized geometry of the excited state. IC stands for internal conversion and CT stands for conformation transformation. Excitation and radiative processes are marked by a solid arrow and the non-radiative processes are marked by dotted arrows.

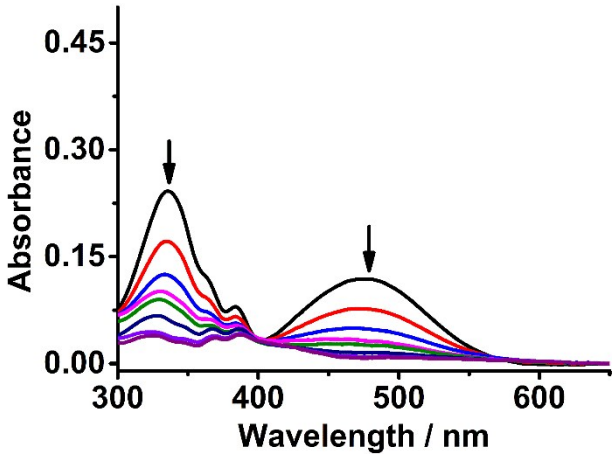

Figure S14. The UV-Vis absorption spectra of probe **XQ-1** (20 μM) with various amounts of $^1O_2$ (0-0.6 mM). The $^1O_2$ was generated from a Na_2MoO_4/H_2O_2 system.

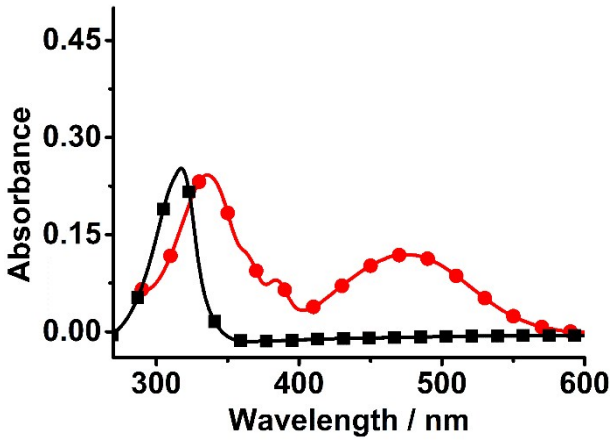

Figure S15. The UV-Vis absorption spectra of probe **XQ-1** (20 μM) (●) and *N*-ethyl-2-methylquinolinium iodide **3** (20 μM) (■).

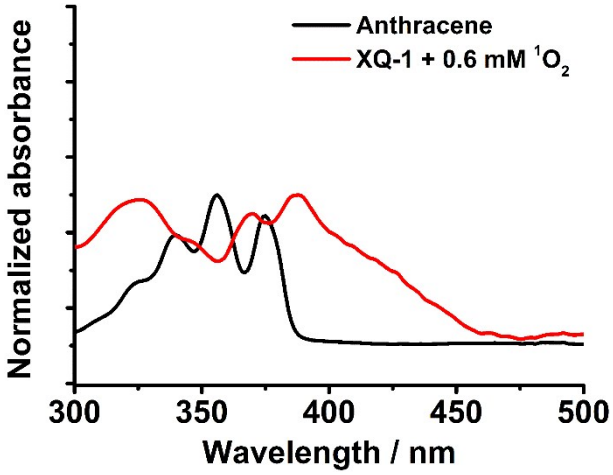

Figure S16. The normalized absorption spectra of probe **XQ-1** (20 μM) + 0.6 mM $^1O_2$ and anthracene **4**. The $^1O_2$ was generated from a Na_2MoO_4/H_2O_2 system.

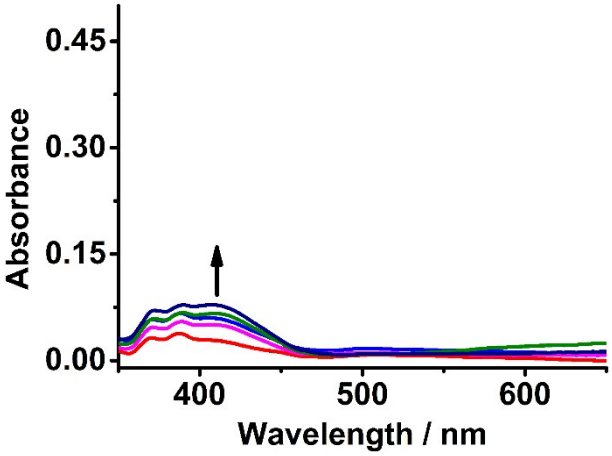

Figure S17. The UV-Vis absorption spectra of probe **XQ-1** (20 μM) with various amounts of $^1O_2$ (0.6 mM-50 mM). The $^1O_2$ was generated from a Na_2MoO_4/H_2O_2 system.

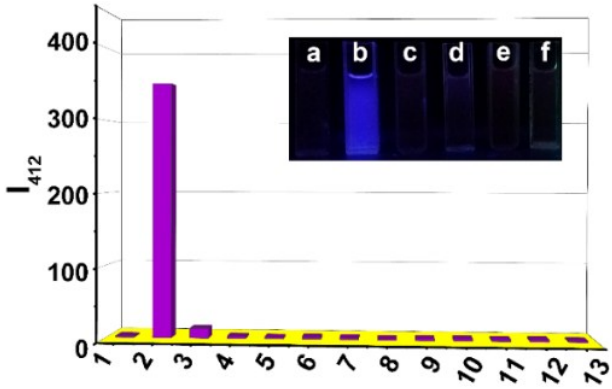

Figure S18. Fluorescence response (λ_{em} = 412 nm, λ_{ex} = 368 nm) of the probe **XQ-1** (20 μM) toward 0.6 mM various analytes: 1) Blank; 2) $^1O_2$; 3) NaClO; 4) H_2O_2; 5) ·OH; 6) NO; 7) GSH; 8) Cys; 9) Mg^{2+}; 10) Fe^{2+}; 11) Fe^{3+}; 12) Cu^{2+}; 13) Zn^{2+}. Inset: the visual fluorescence color of probe **XQ-1** in the presence of 0.6 mM various analytes: a) blank; b) $^1O_2$; c) H_2O_2; d) ·OH; e) Fe^{3+}; f) Zn^{2+}. The $^1O_2$ was generated from Na_2MoO_4/H_2O_2 system.

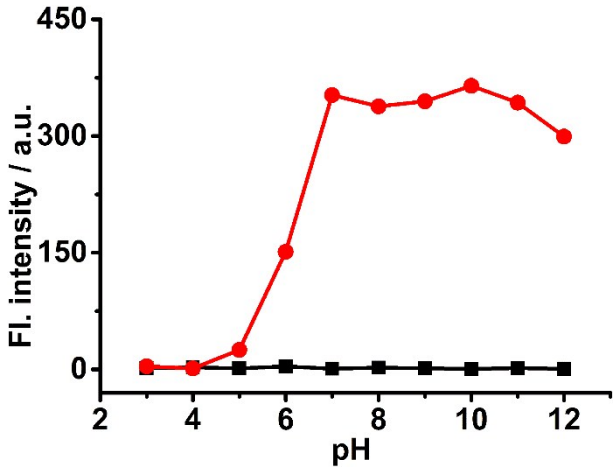

Figure S19. The fluorescence intensity response (λ_{em} = 412 nm, λ_{ex} = 368 nm) of probe **XQ-1** (20 μM) in 50 mM potassium phosphate buffer/ethanol (1:1 v/v) at different pH condition before (■) and after (●) treatment with $^1O_2$. The $^1O_2$ was generated from photoirradiation of co-dissolved **TMPyP4** (5 μM) for 80 seconds.

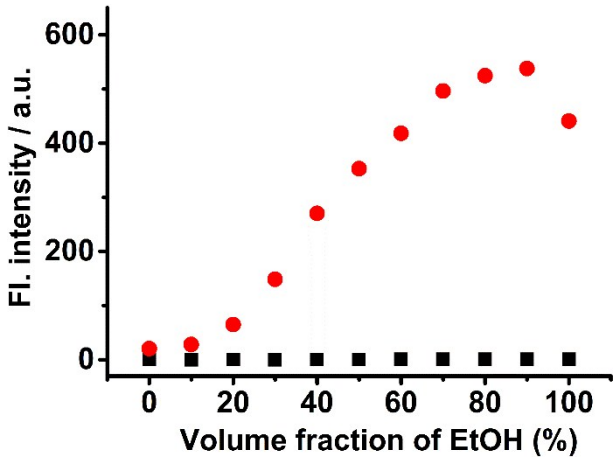

Figure S20. Variation in the fluorescence intensity of probe **XQ-1** (20 μM) as recorded in the presence (●) or absence (■) of $^1O_2$ as a function of the volume fraction of EtOH. The $^1O_2$ was generated from photoirradiation of co-dissolved **TMPyP4** (5 μM) for 80 second.

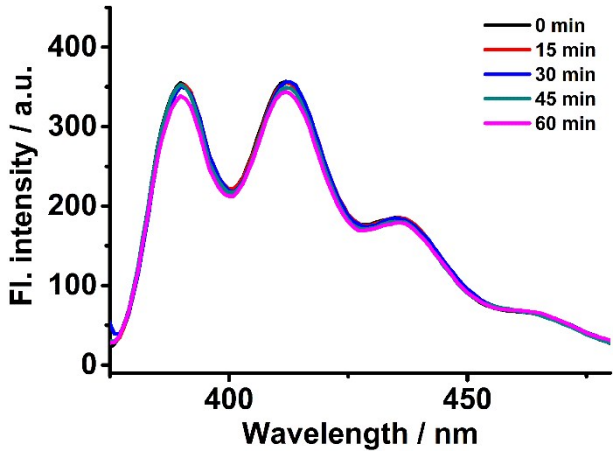

Figure S21. Probe **XQ-1** (20 μM) was reacted with 0.6 mM $^1O_2$ (the $^1O_2$ was generated from a Na_2MoO_4/H_2O_2 system), and then the solution was continuously irradiated with a white LED lamp (150 mW/cm^2). The fluorescence emission spectra in blue channel (λ_{ex} = 368 nm) was recorded at different time interval.

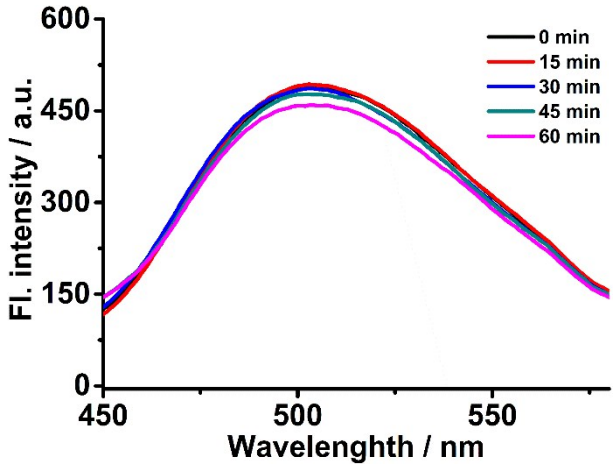

Figure S22. Probe **XQ-1** (20 μM) was reacted with 50 mM $^1O_2$ (the $^1O_2$ generated from a Na_2MoO_4/H_2O_2 system), and then the solution was continuously irradiated with a white LED lamp (150 mW/cm^2). The fluorescence emission spectra in green channel (λ_{ex} = 420 nm) was recorded at different time interval.

11. Kinetic Studies

The reaction rate constant of probe **XQ-1** with $^1O_2$ was estimated under *pseudo*-first-order kinetic conditions (20 μM probe **XQ-1** with 0.6 mM $^1O_2$ or 20 μM probe **XQ-1** with 50 mM $^1O_2$). The reactions of probe **XQ-1** with 0.6 mM $^1O_2$ was monitored by using the fluorescence intensity at 412 nm (Fig. S23a), and the reactions of probe **XQ-1** with 50 mM $^1O_2$ was monitored by using the fluorescence intensity at 506 nm (Fig. S24a). The *pseudo*-first-order rate constant was determined by fitting the fluorescence intensities of probe **XQ-1** to the *pseudo*-first-order equation:[9]

$$\ln[(I_{max} - I_t) / I_{max}] = -k't$$

where I_t and I_{max} are the fluorescence intensities at 412 nm or 506 nm at time t and the maximum value obtained after the reaction was completed. k' is the *pseudo*-first-order rate constant. Fig. S23b and Fig. S24b are the *pseudo*-first-order plot for the reaction of probe **XQ-1** with 0.6 mM $^1O_2$ and 50 mM $^1O_2$, respectively. The negative slope of the line provides *pseudo*-first-order rate constant: *k'*.

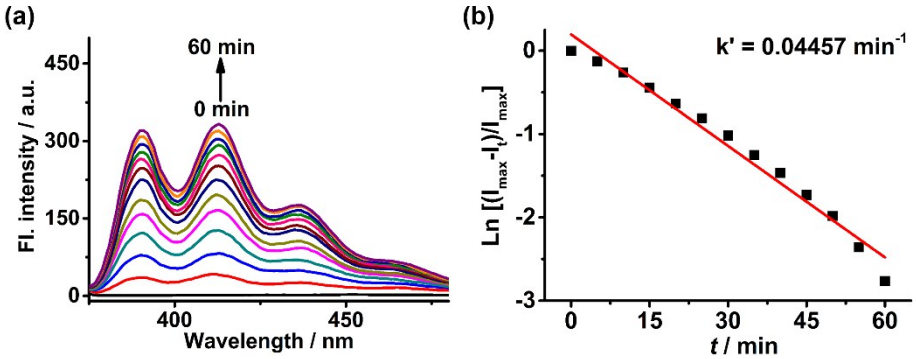

Figure S23. (a) Fluorescence spectra of probe **XQ-1** (20 μM) incubated with 0.6 mM $^1O_2$ in blue channel (λ_{ex} = 368 nm) for 0-60 min. (b) *Pseudo*-first-order kinetic plot of probe **XQ-1** (20 μM) reacted with 0.6 mM $^1O_2$. Slope= - 0.04457 min^{-1}.

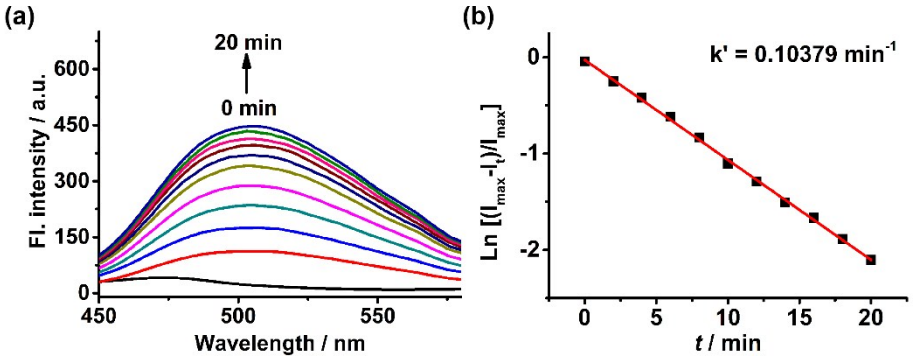

Figure S24. (a) Fluorescence spectra of probe **XQ-1** (20 μM) incubated with 50 mM $^1O_2$ in green channel (λ_{ex} = 420 nm) for 0-20 min. (b) *Pseudo*-first-order kinetic plot of probe **XQ-1** (20 μM) reacted with 50 mM $^1O_2$. Slope= - 0.10379 min^{-1}.

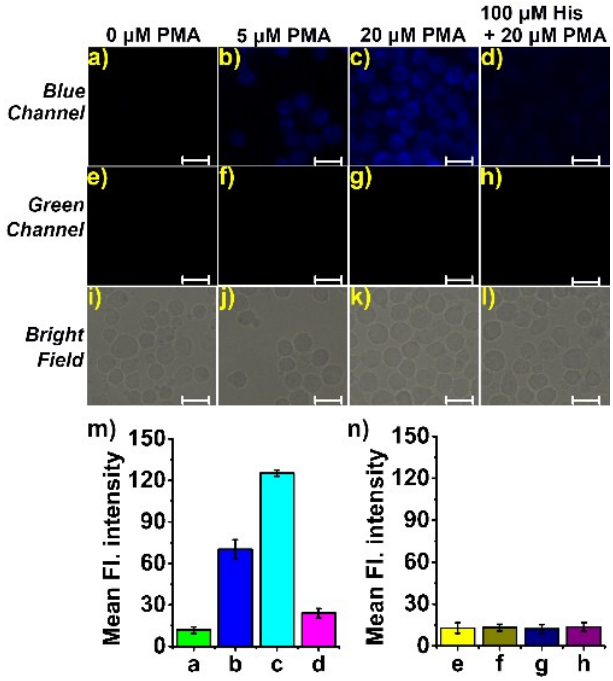

Figure S25. The fluorescence image of probe **XQ-1** detecting endogenous $^1O_2$ in RAW 264.7 macrophage cells. (a)-(c): The fluorescence image in blue channel of the cells stained with 2 μM **XQ-1** in presence of 0 μM, 5 μM, and 20 μM PMA, respectively; (d): The fluorescence image in blue channel of the cells pre-treated with 100 μM His, and then stained with 2 μM **XQ-1** in the presence of 20 μM PMA; (e)-(h): The fluorescence imaging in green channel of the cells corresponding to (a)-(d); (i)-(l): The bright field images of the cells corresponding to (a)-(d); (m)-(n): Quantification of mean fluorescence intensity in (a)-(d) and (e)-(h), respectively. The scale bar in (a)-(l) is 20 μm.

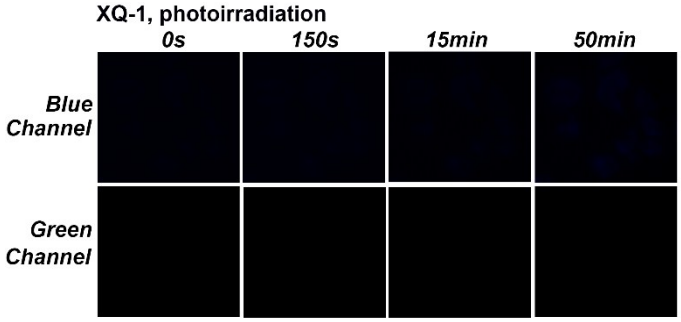

Figure S26. The fluorescence image in the blue channel and green channel of the PC12 cell incubated with 2 μM probe **XQ-1**, and with a continuous 405 nm laser photoirradiation for 0 s, 150 s, 15 min, and 50 min.

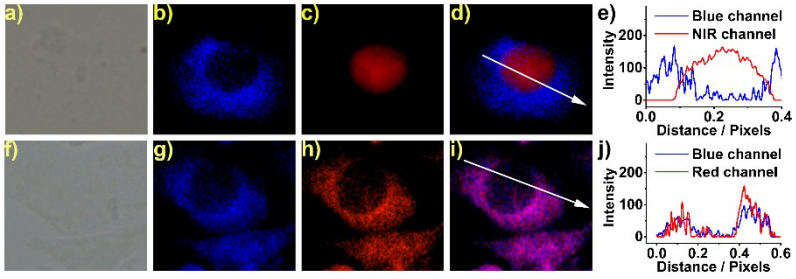

Figure S27. Fluorescence imaging of PC12 cells co-stained with probe **XQ-1** (2 μM) and nuclear stain DRAQ5 (1 μM), or probe **XQ-1** (2 μM) and MitoTracker Orange (0.5 μM). The PC12 cells were incubated with 5-ALA (150 μg ml^{-1}) for 12 hours to biosynthesize photosensitizer PpIX. Then, the cells were stained with probe **XQ-1** (2 μM) for 30 min. After washed with PBS for three times, the cells were further stained with DRAQ5 (1 μM) or MitoTracker Orange (0.5 μM). Upon irradiated with 405 nm laser for 150 s, the fluorescence imaging was acquired. (a-c): Bright field, blue (λ_{em} = 420-450 nm), and NIR (λ_{em} = 670-700 nm) images of PC12 cells co-stained with probe **XQ-1** and nuclear stain DRAQ5. (d): The overlay image of (b) and (c). (e): Intensity profile of regions of interest (ROIs) in the co-stained PC12 cells as indicated by the white arrows in (d). (f-h): Bright field, blue (λ_{em} = 420-450 nm), and red (λ_{em} = 570-610 nm) images of PC12 cells co-stained with probe **XQ-1** and MitoTracker Orange. (i): the overlay image of (g) and (h). (j): Intensity profile of regions of interest (ROIs) in the co-stained PC12 cells as indicated by the white arrows in (i).

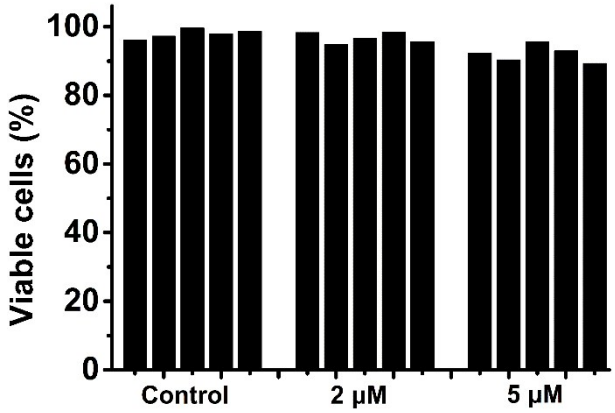

Figure S28. Cytotoxicity of probe **XQ-1** in cultured PC12 cells. The cells were incubated with probe **XQ-1** at 2 and 5 μM for 24 h (n = 5). The cell viability was measured by MTT assay, and the data are reported as the percentage viable cells relative to untreated cells.

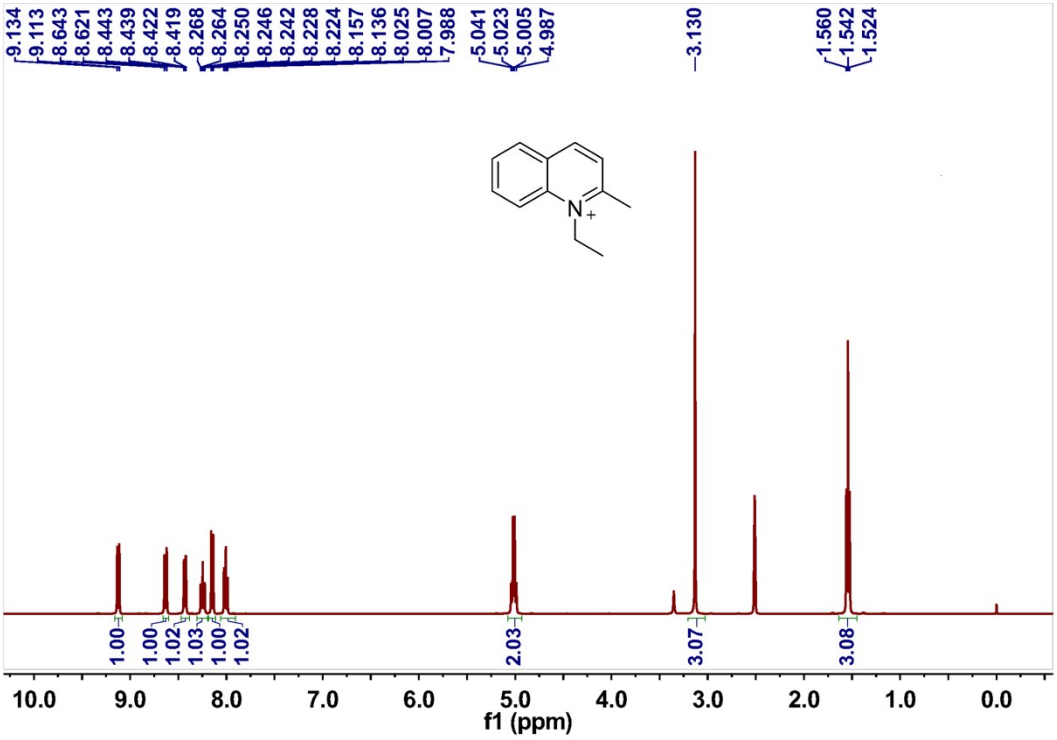

Figure S29. The ^{1}H NMR spectra of **3**.

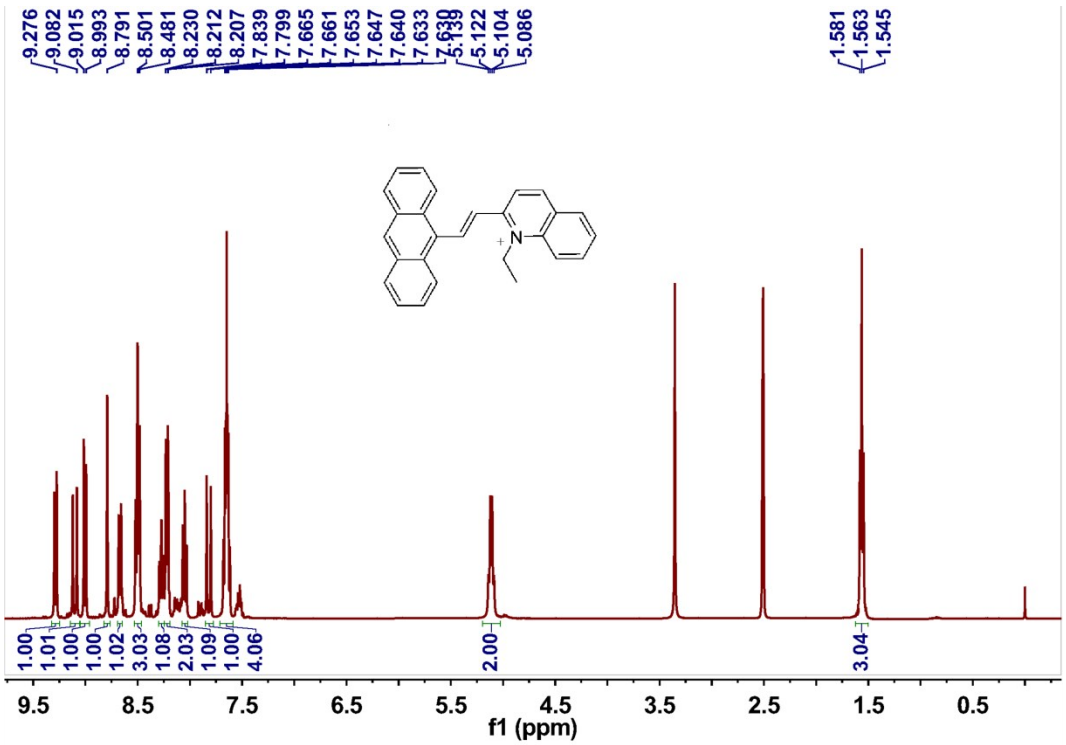

Figure S30. The ^{1}H NMR spectra of **XQ-1**.

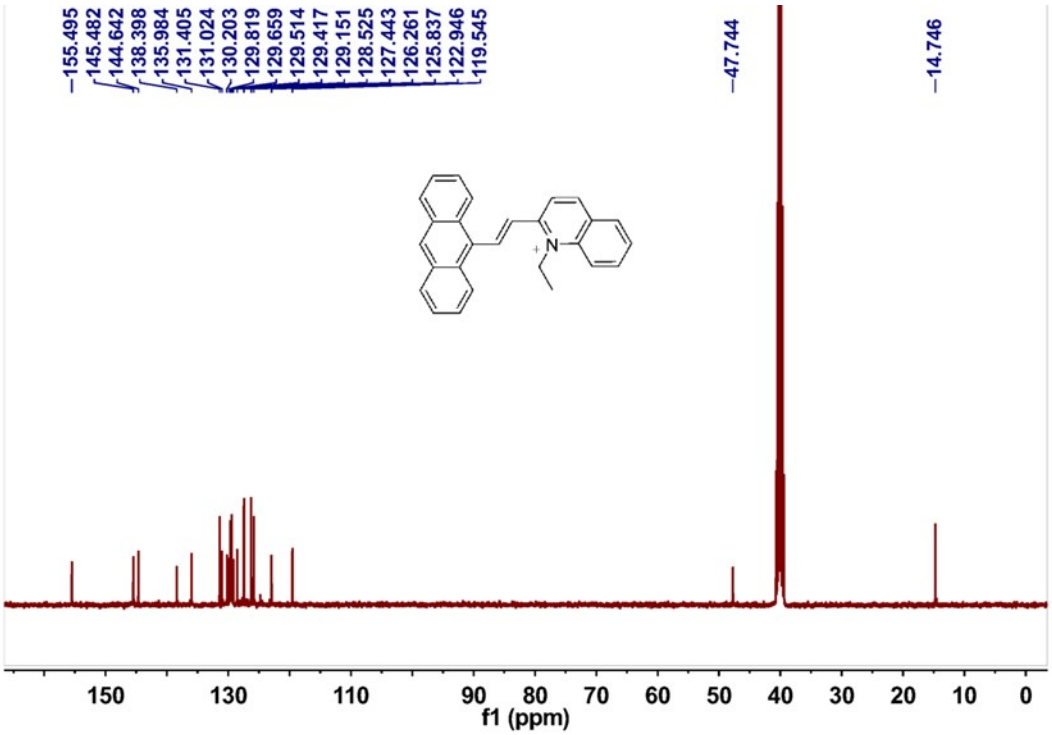

Figure S31. The ^{13}C NMR spectra of **XQ-1**.

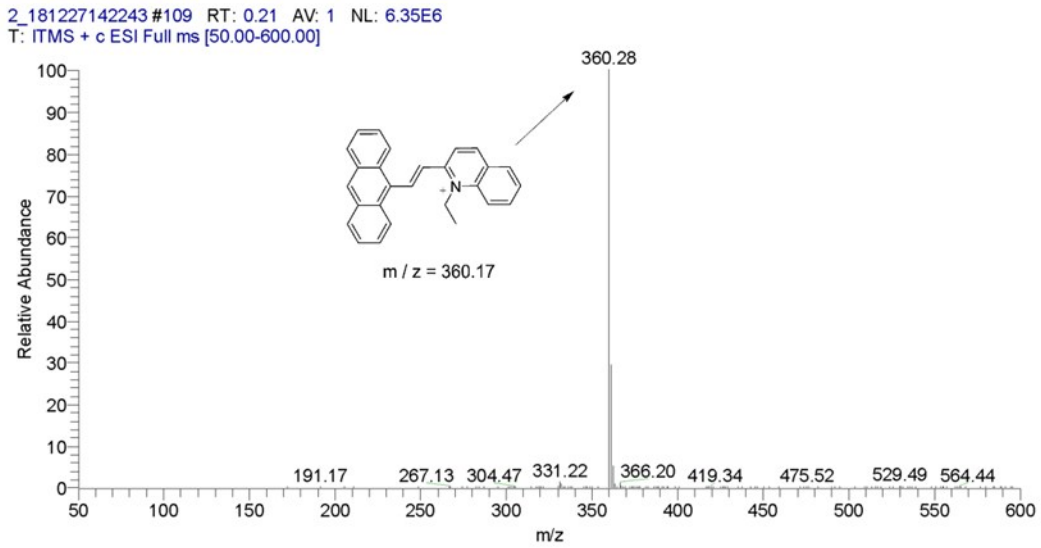

Figure S32. The ESI-Ms spectra of **XQ-1**.

References:

1. J. Aubry and B. Cazin, *Inorg. Chem.*, 1988, **27**, 2013.
2. S. Kim, T. Tachikawa, M. Fujitsuka and T. Majima, *J. Am. Chem. Soc.*, 2014, **136**, 11707.
3. K. Setsukinai, Y. Urano, K. Kakinuma, H. J. Majima and T. Nagano, *J. Biol. Chem.*, 2003, **278**, 3170.
4. (a) Z. N. Sun, F. Q. Liu, Y. Chen, P. K. Tam and D. Yang, *Org. Lett.*, 2008, **10**, 2171; (b) Y. K. Yang, H. J. Cho, J. Lee, I. Shin and J. Tae, *Org. Lett.*, 2009, **11**, 859.
5. F. P. Schwarz and S. P. Wasik, *Anal. Chem.*, 2002, **48**, 524.
6. (a) A. Ajayaghosh, P. Carol and S. Sreejith, *J. Am. Chem. Soc.*, 2005, **127**, 14962; (b) S. Fery-Forgues and D. Lavabre, *J. Chem. Educ.*, 1999, **76**, 1260; (c) C. A. Parker and W. T. Rees, *Analyst*, 1960, **85**, 587.
7. B. Zhu, C. Gao, Y. Zhao, C. Liu, Y. Li, Q. Wei, Z. Ma, B. Du and X. Zhang, *Chem. Commun.*, 2011, **47**, 8656.
8. M. J. Frisch, G. W. Trucks, H. B. Schlegel, G. E. Scuseria, M. A. Robb, J. R. Cheeseman, G. Scalmani, V. Barone, B. Mennucci, G. A. Petersson, H. Nakatsuji, M. Caricato, X. Li, H. P. Hratchian, A. F. Izmaylov, J. Bloino, G. Zheng, J. L. Sonnenberg, M. Hada, M. Ehara, K. Toyota, R. Fukuda, J. Hasegawa, M. Ishida, T. Nakajima, Y. Honda, O. Kitao, H. Nakai, T. Vreven, J. A. Montgomery, Jr., J. E. Peralta, F. Ogliaro, M. Bearpark, J. J. Heyd, E. Brothers, K. N. Kudin, V. N. Staroverov, T. Keith, R. Kobayashi, J. Normand, K. Raghavachari, A. Rendell, J. C. Burant, S. S. Iyengar, J. Tomasi, M. Cossi, N. Rega, J. M. Millam, M. Klene, J. E. Knox, J. B. Cross, V. Bakken, C. Adamo, J. Jaramillo, R. Gomperts, R. E. Stratmann, O. Yazyev, A. J. Austin, R. Cammi, C. Pomelli, J. W. Ochterski, R. L. Martin, K. Morokuma, V. G. Zakrzewski, G. A. Voth, P. Salvador, J. J. Dannenberg, S. Dapprich, A. D. Daniels, O. Farkas, J. B. Foresman, J. V. Ortiz, J. Cioslowski and D. J. Fox, *Journal*, 2013.
9. (a) T. J. Dale and J. Rebek, Jr., *J. Am. Chem. Soc.*, 2006, **128**, 4500; (b) Y. D. Lin, Y. S. Pen, W. Su, K. L. Liau, Y. S. Wen, C. H. Tu, C. H. Sun and T. J. Chow, *Chem. Asian J.*, 2012, **7**, 2864.